

FAR-ULTRAVIOLET OBSERVATIONS OF THE NORTH ECLIPTIC POLE WITH *SPEAR*

ERIC J. KORPELA¹, JERRY EDELSTEIN¹, JULIA KREGENOW¹, KAORI NISHIKIDA¹, KYOUNG-WOOK MIN², DAE-HEE LEE^{2,3},
KWANGSUN RYU², WONYONG HAN³, UK-WON NAM³, JANG-HYUN PARK³

Accepted for publication in ApJ Letters on 19 December 2005

ABSTRACT

We present *SPEAR/FIMS* far-ultraviolet observations near the North Ecliptic Pole. This area, at $b \sim 30^\circ$ and with intermediate HI column, seems to be a fairly typical line of sight that is representative of general processes in the diffuse ISM. We detect a surprising number of emission lines of many elements at various ionization states representing gas phases from the warm neutral medium (WNM) to the hot ionized medium (HIM). We also detect fluorescence bands of H₂, which may be due to the ubiquitous diffuse H₂ previously observed in absorption.

Subject headings: ISM: general, ISM: lines and bands, ultraviolet: ISM

1. INTRODUCTION

The North Ecliptic Pole (NEP) is a region of the sky with no obviously unusual features. Many prior space-missions (*Einstein*, *ROSAT*, *COBE*, *IRAS*, etc.) have conducted deep surveys of this region. Several ground based surveys have also concentrated on this region as a complement to the space-based surveys (Labov et al. 1989; Elvis et al. 1994). Its location at moderate galactic latitude ($b=+29^\circ$) places it clear of the bright stars of the galactic plane. In this region, the Galactic N(HI) varies from about $2 \times 10^{20} \text{ cm}^{-2}$ to $8 \times 10^{20} \text{ cm}^{-2}$ which corresponds to an dust opacity of $\tau_{\text{dust}} = 0.6\text{--}2.3$ at 1032\AA (Sasseen et al. 2002) or $\tau_{\text{dust}} = 0.3\text{--}1.4$ at 1550\AA (Savage & Mathis 1979).

The Spectroscopy of Plasma Evolution from Astrophysical Radiation (*SPEAR*) instrument, designed for observing emission lines from the diffuse ISM was launched in late 2003. *SPEAR* is a dual-channel FUV imaging spectrograph (short- λ (S) channel 900 - 1150 \AA , long- λ (L) channel 1350 - 1750 \AA) with $\lambda/\Delta\lambda \sim 550$, with a large field of view (S: $4.0^\circ \times 4.6'$, L: $7.5^\circ \times 4.3'$) imaged at $10'$ resolution. See Edelman et al. (2005a,b) for an overview of the instrument, mission, and data analyses. *SPEAR* sky-survey observations consist of sweeps at constant ecliptic longitude from the NEP to the south ecliptic pole through the anti-solar point. The duration of each sweep varies between 900 and 1500 s. Each survey scan includes the region near the north and south ecliptic poles resulting in large exposure times in these regions. We report on deep *SPEAR* observations of FUV emission spectra from a 15° radius region centered on the NEP.

2. OBSERVATIONS AND DATA REDUCTION

The NEP data analyzed here include sky-survey and pointed observations that occurred between 8 November 2003 to 10 November 2004. To remove times of high background and bright stars from the data set, we have excluded times during which the count rate exceeds 100

s^{-1} . (In comparison, a typical photon count rate is $\lesssim 20 \text{ s}^{-1}$.) Because stars transit the instrument slit in ~ 5 s during survey sweeps, this results in minimal loss of observing time. The area of sky lost due to a star is similar to the instrument imaging resolution across the slit width ($\sim 10' \times 5'$). See Edelman et al. (2005a) for a description of the data reduction pipeline.

To further remove stellar contamination from our dataset, we excluded locally intense spatial bins ($\sim 30\%$ of the viewed area), defined to have $\gtrsim 3 \times$ the median count rate. This level corresponds with a slope change in the histogram of the log count rate, indicative of a difference in distribution of scattered vs direct starlight. Inclusion of unresolved starlight should not be a factor other than to raise emission-line determination errors. To obtain the highest sensitivity possible, we have binned the entire dataset into a single spectrum including a total of 3.5×10^5 counts over an effective full-slit exposure of 13.5 ks.

3. SPECTRAL MODELING

The raw *SPEAR* spectrum is composed of many components: detector background, dust-scattered stellar continua, direct and instrumentally scattered airglow, and IS atomic and molecular emission. To model a spectrum we simultaneously fit all of the components to the observed spectrum.

The spectral shape is distorted by the detector electronics and by the data processing pipeline. These distortions appear as fluctuations in a flat-field image. Any broad-band component used in our model spectrum must be multiplied by this nonlinearity function. (Korpela et al. 2003; Rhee et al. 2002).

Both S and L are affected by instrumental background due to cosmic rays, radioactive decay within the detector, and thermal charged particles entering the instrument. These sources of background are relatively uniform across the face of the detectors. Although the charged particle rate can change with time and orbital position, the positional distribution of these background events is dominated by static fields within the instrument and is relatively constant. A sum of many shutter-closed dark exposures multiplied by a rate factor can be used to model this contribution to the spectrum.

In L, the largest broad-band spectral component is

¹ Space Sciences Laboratory, University of California, Berkeley, CA 94720-7450; korpela@ssl.berkeley.edu

² Korea Advanced Institute of Science and Technology, 305-701, Daejeon, Korea

³ Korea Astronomy and Space Science Institute, 305-348, Daejeon, Korea

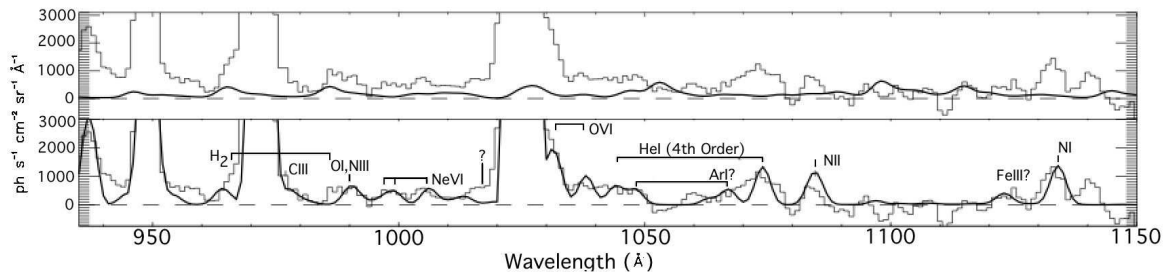


FIG. 1.— S channel H₂ and line emission models. Upper panel: best fit H₂ fluorescence model is shown against the residuals following subtraction of the continuum/background model. The H₂ features’ positions are well predicted, but their ratios are not. The H₂ is oversubtracted near 1100 Å and undersubtracted shortward of Ly β λ 1026. Features at λ < 1000 Å are underpredicted. Lower Panel: The best fit atomic line spectrum is plotted against the residuals following subtraction of the H₂ spectrum. Probable H₂ features and several as yet unidentified features remain throughout the band.

dust scattered stellar continua. We model the input spectrum to the dust scattering process as a sum of spectra for upper main sequence (UMS) stars. Each spectrum is weighted by using a power law UMS luminosity function ($dN/dM_v \propto 10^{\alpha M_v}$, where M_v is the absolute magnitude and dN/dM_v is the volume density of stars per unit magnitude) and a dilution factor dependent upon the weighted mean distance of the stars. The spectral sum is multiplied by a dust opacity scaled to a variable $N(HI)$ and by a dust albedo function (Draine 2003) with a variable total dust surface area. The best fits for this function typically occur very near to the measured UMS luminosity function with $\alpha \sim 0.2$ (Reed 2001). Because the stellar features in this spectrum cannot be directly measured, there may be some bias in our measurements of the overlying resonance lines (CIV λλ 1548,1551, OVI λλ 1032,1038, SiIV λλ 1394,1403, etc.) of order ~ 1000 ph s⁻¹ cm⁻² sr⁻¹ (LU). We include this effect in our error analysis. Our best fit continuum, which could include unresolved stars, is $300 \pm_{50}^{140}$ ph s⁻¹ cm⁻² sr⁻¹ Å⁻¹ (CU) in L. In S, due to its lower sensitivity and higher non-astrophysical background, we are only able to place a statistical upper limit of 1200 CU. However, given the wavelength dependence of the dust albedo, we expect that the true S astrophysical continuum is no higher than in L.

We first attempted to fit atomic line emission by using linear combinations of collisional ionization equilibrium (CIE) plasma models with a limited abundance gradient vs T . We attribute this method’s lack of success to photoexcitation of resonance lines, non-CIE effects and abundance variations that are not T related. To fit the line emission we have, instead, fit the spectrum of each species separately with a per-species intensity and T parameter. The emission line spectra are convolved with a λ -dependent Gaussian to model the instrument spectral resolution. We use the atomic parameters of CHIANTI (Young et al. 2003) to determine the spectrum of the species vs T . This spectrum is then normalized and multiplied by the intensity parameter. When CHIANTI parameters are not available for a species, we use a spectrum calculated using the NIST Atomic Spectra Database.

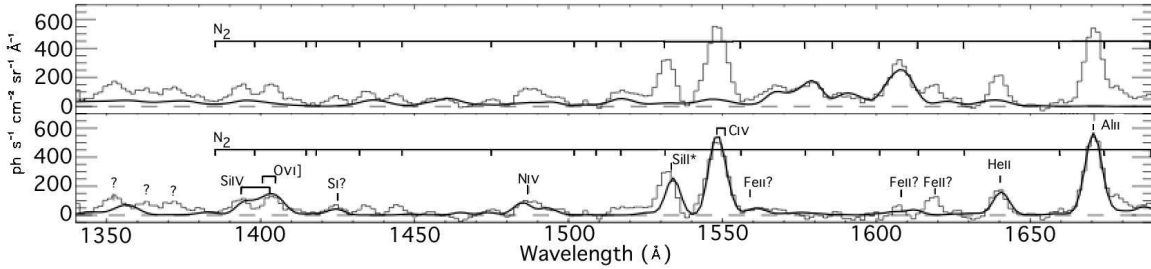
We then consider the effects of self-absorption of spectral resonance lines. In the case of highly ionized species we assume all lines are optically thin. We also assume this to be the case for species that would be com-

pletely photoionized in the WNM (ionization potential (IP) <13.6 eV). For species which are likely to be abundant in the WNM and warm ionized medium (WIM), (IP $\gtrsim 13.6$ eV) we assume that resonance lines are optically thick ($\tau > 10$) and that the distances to the illuminating stars are large compared to the $\tau = 1$ surface. In cases where the ground state is split, absorbed resonance line photons will be converted to the excited state, greatly changing the relative contributions in the multiplet. We model this by attenuating the ground state transition by a large factor. We will develop a more accurate way of treating these optical depth effects in future work.

4. DISCUSSION

The spectrum of the bright Lyman-series geocoronal emission, easily visible in Fig. 1, can be modeled using a temperature and total line flux. The largest S broadband component is scattered geocoronal Ly α λ 1216 emission. This line occurs in the bandpass gap between S and L. L is immune to Ly α contamination because it includes a CaF₂ filter which is very nearly opaque to Ly α radiation. We fit the S scattering with two components, an exponential scatter $\propto \exp(-|\lambda - \lambda_0|/\alpha)$ with $\alpha \sim 200$ Å, and an isotropic component. The scattering, summed over the entire spectrum, is $\sim 0.08\%$ of a ~ 5 kRy Ly α incident flux. Because the Ly α transition is optically thick, and because the scattering fractions are independent parameters, we fix the estimated incident Ly α flux at $1100\times$ the Ly β flux which helps the solution to converge. While the fractional scatter and exponential width of these components are free parameters in our spectral model, the values we obtain vary little from one dataset to the next.

Our model includes spectral features of atmospheric OI, CI, and NI that are much fainter than when seen in day-time observations (e.g. *FUSE*), as *SPEAR* only observes during orbital eclipse. We detect a spectral feature near 990 Å that is consistent with the OI λ 989 transition. However, this feature may be blended with NIII λ 990. If the entirety of the 990 Å feature is due to OI, the lack of detectable OI λ 1356 emission would indicate $T > 10^{3.6}$ K, which is plausible for interstellar OI. We do detect OI λ 1356 in data that is not count rate filtered. The other possibility is that the 990 Å is due to OI at $T \sim$ few hundred K which seems unlikely even for atmospheric OI. The most likely explanation for the lack of any detection of OI emission at $\lambda \neq 990$ Å is that a large portion, if not all, of the 990 Å emission is due to NIII.

FIG. 2.— L channel H_2 and line emission models.

We detect relatively strong emission from H_2 fluorescence bands even in this region of intermediate $N(HI)$. This is not entirely surprising since absorption due to H_2 is a ubiquitous feature of FUV spectra taken by *FUSE*. (Shull et al. 2000) We fit these features by using interpolation between a sparse grid of H_2 models (B. Draine 2004, private communication). The upper panels of Figs. 1 & 2 show the best fit H_2 model plotted against the residuals of the spectrum following background, continuum, and scattering subtraction. We detect H_2 emission features in both spectral bands. In S we detect the H_2 $\lambda\lambda$ 965 band (to the left of the HI λ 972 line) and the H_2 $\lambda\lambda$ 986 band (to the left of the OI, NIII $\lambda\lambda$ 989 feature). The H_2 $\lambda\lambda$ 1053 and $\lambda\lambda$ 1097 bands are not detected at any significance. In L, H_2 provides contributions throughout the spectrum. We attribute the triple peaked band structure between 1350 and 1380 Å, the peak near 1440 Å, the broad features $\lambda\lambda$ 1520-1530, $\lambda\lambda$ 1570-1590, and the peak near 1608 Å to H_2 . Note that these features are not well fit by our H_2 model. It is not surprising that our sparse linear model with a single dust absorption column does not fit these data since the observed emission derives from many lines of sight with varying illumination, gas temperatures and absorbing columns. In Figs. 1 & 2, lower panels we show the residual spectrum following subtraction of the H_2 component.

We see intriguing indications of N_2 fluorescent emission, most notably the features at 1434 Å, 1445 Å, 1475 Å, and 1660 Å. *FUSE* has detected absorption due to N_2 along some sight-lines, albeit at shorter wavelengths (Knauth et al. 2004). We cannot yet discount the possibility that these N_2 features are atmospheric, as near the magnetic poles, N_2^+ can be transported to high altitude. Further study to determine whether the N_2 emission varies with spacecraft orbital position or with galactic latitude of the observation should resolve this question. If confirmed as astrophysical, this would be the first detection of fluorescent N_2 emission from the diffuse ISM.

SPEAR has discovered some surprising spectral features, such as the resonance lines of the singly ionized species, SiII and AlII. The AlII feature at 1671 Å very nearly overlies the OIII] $\lambda\lambda$ 1665 which we do not detect in this dataset. In a lower resolution instrument these spectral features could be blended resulting in confusion of the OIII] and AlII emission. We think it is likely that at least some of the prior claimed detections (Martin & Bowyer 1990) of OIII] were in fact misidentified detections of AlII $\lambda\lambda$ 1671. We attribute the feature

TABLE 1
OBSERVED WARM/HOT ISM EMISSION LINE INTENSITIES

Species	λ Å	I_λ LU ^a	Statistical Error LU	Model Uncertainty LU
OIII]	1667	<500 ^b	—	—
OIV]	1400	1980	±220	±300
OVI	1032,1038	5724	±570	±1100
CIII	977	1260	±270	—
CIV	1548,1551	5820	±280	+0 -1490
SiII*	1532	2430	±200	+630 -0
SiIV	1394,1403	1430	±120	±160
NII	1085	8500	±730	—
NIII	990	<2300	—	—
NIV	1485	1984	±170	±450
AlII	1671	5608	±525	—
HeII	1640	1850	±180	+0 -500
NeVI	999,1005	<4100	—	—

NOTE. — ^aLU=ph s⁻¹ cm⁻² sr⁻¹ ^bUpper limits are 90% confidence

at 1533 Å to the SiII* λ 1533.4 transition into the upper fine structure level of the ground state. The offset between the model feature and the observed line may be due to an uncorrected continuum feature underlying this line (Fig. 3 of Edelman et al. (2005a)). Since SiII is the predominant state of silicon in both the WNM and WIM, the true SiII λ 1526.7 ground state transition is likely to be optically thick and therefore undetectable. Our spectral models are improved by the addition of FeII transitions throughout band, most notably the FeII $\lambda\lambda$ 1564, which fills the gap between CIV $\lambda\lambda$ 1548,1551 and the $\lambda\lambda$ 1570-1590 H_2 band. It is also possible that there is a contribution to the H_2 $\lambda\lambda$ 1600-1620 band due to the FeII $\lambda\lambda$ 1608 resonance lines. These lines have a fairly low oscillator strength and are expected to be optically thin along this line of sight. However, given the low oscillator strength, we expect these lines to be faint compared to the SiII and AlII features.

Emission lines of highly ionized gas expected to be generated in a CIE plasma at HIM temperatures are shown in Table 1. Of these we detect ($> 3\sigma$) CIV λ 977, CIV $\lambda\lambda$ 1548,1551, SiIV $\lambda\lambda$ 1394,1403 and OVI $\lambda\lambda$ 1032,1038. The CIV $\lambda\lambda$ 1549 and SiIV $\lambda\lambda$ 1400 emission overlie prominent stellar absorption features which are likely to be present in the dust-scattered stellar radiation. Since the depth of these features is unknown we set the lower range of our model uncertainty to be the intensity that would be

calculated if there were no continuum feature present.

Many of these emission features are resonance lines (R. J. Reynolds 2005, private communication) and, because of the substantial IS radiation field at these wavelengths, further work will be required to determine whether these lines arise due to collisional excitation in the HIM or due to resonant scattering of the IS radiation field. We believe that the short wavelength lines are less likely to be resonant scatter because the relative intensity of the scattered stellar continuum in the S band is much lower (Korpela et al. 1998).

Our C IV $\lambda\lambda$ 1548,1551 intensity of 5820 ± 280 LU is marginally higher than values for the diffuse ISM reported by Martin & Bowyer (1990). However Martin and Bowyer assumed a featureless continuum rather than a continuum with stellar features. If we make the same assumption our value drops to 4330 ± 210 LU which is more within the range of values they report.

Our O VI $\lambda\lambda$ 1032,1038 intensity of 5724 ± 1100 LU is somewhat higher than the typical value measured by *FUSE* (Shelton 2003). This could be a systematic effect due to the uncertain calibration of the S band. In fact the ratio of the H_2 feature intensities between L and S suggests that we have underestimated the sensitivity of S. Since this is an average over a very large region, it is also possible that the O VI emission is due to several small regions with very high intensity, such as SNR.

The double peaked feature near 1400 Å is a blend of Si IV $\lambda\lambda$ 1393.8,1402.8 and O IV] $\lambda\lambda$ 1400.7,1407.4. The O IV] emission is of great interest because, as a semi-forbidden line, it is not strongly affected by the radiation field, but is a direct indicator of collisional processes. Assuming a 2:1 ratio for the Si IV doublet components, our model determines the O IV] doublet intensity to be 1980 ± 300 LU and the Si IV doublet intensity to be 1430 ± 160 LU.

We detect high stage ions of two noble gases in our spectra, He II $\lambda\lambda$ 1640 and Ne VI $\lambda\lambda$ 999,1005. Although the features corresponding to the Ne VI lines are statistically significant, the poor fit to the underlying H_2 bands prevents us from placing more than an upper limit to these features. Because of the lack of detection of any O I λ 1356, we do not expect any contamination of the He II line with O I λ 1641. The He II line is much brighter than would be expected in a solar abundance CIE model (in ratio to C III and O III). This could be due to depletion of C and O to $\lesssim 0.1$ solar. A depletion of this magnitude would be significantly higher than the accepted values for the ISM.

In Fig. 3 we show equivalent solar abundance emission measure (EM) and limits for several species. The results are not entirely consistent between species. For example higher EM is necessary to explain the Si IV and He II emission than are compatible with the amount of C III emission. The questionable Ne VI detections would indicate EM $10\times$ that suggested by the O VI measurements. The bulk of the inconsistency in Ne VI is likely to be due to undersubtraction of the underlying H_2 . Much of the inconsistency in other lines is likely due to non-CIE effects which are present in gas being heated or cooling

at these temperatures. Some portion of the difference could be due to abundance variations (with ISM depletions of O and C higher than those of Ne, He, and Si), although the suggested depletions are much higher than

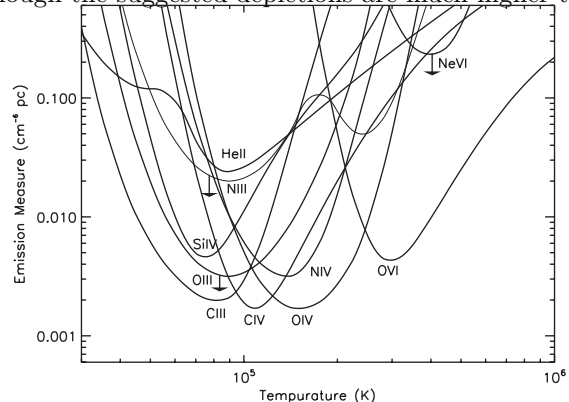


FIG. 3.— Solar abundance emission measure (EM) vs T for detected emission lines and significant upper limits. The lines represent the loci of EM necessary to produce the observed intensities.

the accepted ISM values. In future work we will derive constraints to non-CIE cooling models and abundances using these line ratios.

5. CONCLUSIONS

We have presented the FUV spectra of a 30° region around the NEP. We detect a variety of emission lines from high and low ionization gas. The high ionization lines, taken on a per species basis, are consistent with EM from 0.001 to $0.005 \text{ cm}^{-6} \text{ pc}$ throughout $T = 10^{4.5}$ to $10^{5.5}$ K range. For those few species which have multiple lines in the band, the calculated temperatures tend to fall near the CIE peak abundance for the species. Despite this, a linear combination of CIE models with a restricted abundance vs T gradient does not provide a good fit to the spectrum. This is likely due to non-CIE effects and abundance variations are not directly T related. It is also likely that many lines include some resonantly scattered stellar radiation. Modeling this scattering will be a significant portion of our continued research.

We have discerned line emission from species that are expected to exist in the WNM and WIM. We interpret these lines as resonantly scattered stellar radiation. In the future, we will investigate if spatial variation of the Al II and Si II features can indicate the effect of grain formation and destruction on the gas phase abundances of these elements.

Despite relatively low galactic $N(HI)$ in this direction, we see a substantial amount of H_2 fluorescence. Further modeling of the H_2 fluorescence is necessary to fully understand faint spectral features which could be related to H_2 or due to unrelated atomic lines.

SPEAR/FIMS is a joint project of KASSI & KAIST (Korea) and U.C., Berkeley (USA), funded by the Korea MOST and NASA Grant NAG5-5355.

REFERENCES

Draine, B. T. 2003, *ApJ*, 598, 1017
Edelstein, J., et al. 2005a, *ApJ*, this volume

Edelstein, J., et al. 2005b, *ApJ*, this volume
Elvis, M., Lockman, F. J., & Fassnacht, C. 1994, *ApJS*, 95, 413

- Knauth, D. C., et al. 2004 BAAS, 205.5906
Korpela, E. J., Bowyer, S., & Edelstein, J. 1998, ApJ, 495, 317
Korpela, E. J., et al. 2003, Proc. SPIE, 4854, 665
Labov, S. E., Yan, B. H. W., & Wai, Y. C. 1989, BAAS, 21, 1123
Martin, C., & Bowyer, S. 1990, ApJ, 350, 242
Reed, B. C. 2001, PASP, 113, 537
Rhee, J. G., et al. 2002, JASS, 19, 57
Sasseen, T. P., et al. 2002, ApJ, 566, 267
Savage, B. D., & Mathis, J. S. 1979, ARA&A, 17, 73
Shelton, R. L. 2003, ApJ, 589, 261
Shull, J. M., et al. 2000, ApJ, 538, L73
Young, P. R., et al. 2003, ApJS, 144, 135